Int. J. Electrochem. Sci., 11 **(2016)** 5035 – 5045, doi: 10.20964/2016.06.3

International Journal of ELECTROCHEMICAL SCIENCE
www.electrochemsci.org

Surfactant Effect as Template Agent on the Morphological and Electrochemical Properties of V_2O_5

Fernanda R. Lemos[1], *Leonardo M. da Silva*[2], *Dane T. Cestarolli*[1], *Elidia M. Guerra*[1,*]

[1] Department of Chemistry, Biotechnology and Bioprocess Engineering, Federal University of São João Del Rei, Ouro Branco, MG, Brazil
[2] Department of Chemistry, Federal University of Jequitinhonha and Mucuri Valley, Diamantina-MG, Brazil
[*]E-mail: elidiaguerra@ufsj.edu.br

Received: 19 February 2016 / *Accepted:* 22 March 2016 / *Published:* 4 May 2016

The effect of the release of cetylpyridinium chloride surfactant into the V_2O_5 following the behavior of lithium intercalation into an electrode containing the V_2O_5 film has been investigated. X-ray diffraction patterns indicated formation of a lamellar structure. After the calcination and release of surfactant occurred the formation of an orthorhombic structure. Scanning Electronic Microscopy shows that the route employed for the preparation of an open network V_2O_5 structure was successful. The electrochemical performance of the open network structured material compared with a compact structure of V_2O_5, via sol-gel route as lithium intercalation cathode materials were evaluated. The open network material reaches stability more easily and presents a high total voltammetric charge after several cycles compared with the V_2O_5 xerogel. Lithium intercalation into the V_2O_5 electrode is very influenced by open network surface and surface irregularity, in contrast with the compact surface of the V_2O_5 xerogel.

Keywords: Intercalation reaction; V_2O_5 xerogel; open network; surfactant; electrochemical studies

1. INTRODUCTION

The development and growth of renewable energy has been the focus of an international scenario since there is a need for a replacement of fuels source, such as petroleum, that are finite source and increase the level of environmental pollution with the release of gases that are capable of damaging the ozone layer and aggravate the greenhouse effect [1]. The cleaner energy generation will increase the need for storage in order to supply with costumer demand. For these demands, the rechargeable lithium batteries, compared with alternative battery technologies, renders the choice of

power source [2]. Besides, the demand for clear energy combined with renewable energy has requested a number of studies using transition metal oxides (TMO) because their broad potential application as power source such as solar cell, rechargeable lithium–ion batteries and smart windows [3-5]. TMO are the well-known conventional structures used in lithium batteries forming a lithium metal oxide, generally as a cathode. Among the main materials have been recently studied, it is possible to point out the lithium nickel oxides ($LiNiO_2$), cobalt ($LiCoO_2$), manganese ($LiMn_2O_4$) and vanadium (LiV_2O_5). These cathodes are called mixed conductors due to electronic and ionic conduction are operative [6,7]. The electro-intercalation on TMO are associated with the fact that when these systems are oxidized or reduced electrochemically, the connection oxygen/metal is maintained, i.e., due to its high energy, as well as the occurrence of the electroneutralization process, this process must be accompanied by the cations intercalation in the host network. In rechargeable batteries, it is desirable that the Li^+ ions are to be inserted interstitially within the host structure during discharge, and subsequently released during charging with little or no structural modification of the host material [8-10]. Whittingham, *et al.* published several articles about cathode materials for lithium batteries including the use of vanadium oxides [11,12]. The vanadium pentoxide, V_2O_5, is a TMO that presents a lamellar structure when obtained by sol-gel route. The lamellar structure of V_2O_5 presents a basal spacing of 1.17 nm [13] that make possible the intercalation of several guest materials such as polymers [14,15] and surfactants [7,16]. However, some drawbacks can occur which affect the final electrochemical properties. It is possible to point out examples as the charge density is low due to the low conductivity of the TMO and the cyclic life of the material decrease after the first ten cycles causing a collapse of the structure during the long-term charge–discharge cycle [17]. In order to improve the electrochemical properties of TMO, different structures and synthetic routes are required to improve the Li^+ insertion kinetic. The kinetic of ion insertion is limited by low active sites in V_2O_5 obtained via sol-gel. However, to reduce the length of the diffusion path is necessary a higher quantity of active sites by porous network [14]. Thus, to obtain a higher quantity of active sites into the material is necessary to use a process called an intercalation reaction that containing, for example, V_2O_5 matrix/surfactant species hybrid material, followed the release of the surfactant by thermal treatment [18]. In this context, our interest is to investigate the effect of the porosity obtained by release of cetylpyridiniun chloride (CPC) from vanadium pentoxide matrix. This material was used as host cathode matrix on the Li^+ insertion/deinsertion process. To this end, voltammetric studies were carried out as a function of the total voltammetric charge.

2. EXPERIMENTS

2.1. Preparation of the V_2O_5/CPC and porous V_2O_5

The porous material was prepared from calcination of surfactant, CPC into V_2O_5 xerogel. As the first step, the vanadium pentoxide gel, $V_2O_5nH_2O$, was prepared from sodium metavanadate ($NaVO_3$, 99%) by the ion exchange method (ion-exchange resin Dowex-50x8). It was obtained a decavanadic from 0.10 mol L^{-1} of a $NaVO_3$ aqueous solution through a cationic ion-exchange resin.

After put to rest at room temperature for 2 weeks, the fresh HVO_3 solution was polymerized, leading to a viscous red V_2O_5 gel. In 5 mL of V_2O_5, via sol-gel, were added, separately, 0.1 mol L^{-1} and 0.2 mol L^{-1} of CPC at room temperature under constant stirring for 48 h. The resulting brown suspensions were cast into a film form by evaporation of water at room temperature on a substrate for analyses. The films were named as VC1 and VC2 for V_2O_5/CPC in 0.1 mol L^{-1} and V_2O_5/CPC in 0.2 mol L^{-1} of surfactant, respectively.

The porous materials were prepared for calcination of VC1 and VC2. The calcination temperature used was based on thermogravimetric analyses. After calcination of VC1 and VC2 in 350^o C, the materials were named as: V1 and V2, respectively.

2.2. Equipment and procedure

The thermogravimetric data were registered on a Thermal Analyst equipment, model DTG-60H, Shimadzu, in air atmosphere, at a heating rate of 10 C min^{-1}. The X-ray diffraction (XRD) data were recorded on a XRD-6000 from Shimadzu, using a graphite monochromator and CuK_α emission lines (1.541 Å, 40 kV, 40 mA). To this end, samples in the film form and deposited onto a glass plate were employed, and the data were collected at room temperature over the range $2° \leq 2\theta \leq 50°$, with a step of 0.020°. Scanning electron microscopy (SEM) was carried out on a TESCAN microscope VEGA3 LMH model operating at 30 kV. A thin gold coating (≈ 20Å) was applied to the sample using a Sputter Coater – Balzers SCD 050.

Voltammograms were measured using an μAUTOLAB Type III (Metrohm) potentiostat/galvanostat interfaced with a computer. A platinum substrate was used in order to support the samples (electrodes). The mass of V1 and V2 sample materials was deposited on the electrode surface (3.0 mg) and dried at room temperature (24 °C). The supporting electrolyte was 1.0 mol L^{-1} $LiClO_4$ in acetonitrile medium.

3. RESULTS AND DISCUSSION

The TG-DTG curves of VC1 and VC2 are showed in Fig. 1 and 2. For both VC1 and VC2 is observed a first weight loss between 90 to 220 °C relating to the removal of water adsorved. The second stage of weight loss, between 220 to 370 °C and 220 to 325 °C for VC1 and VC2, respectively, correspond to the major weight loss stage. This stage involves the loss of coordinated/interlayer water molecules present in the hybrid materials, as well as the decomposition of CPC. Finally, the last step, above 350 °C is attributed to transformation of the vanadium pentoxide xerogel into crystalline vanadium pentoxide [19]. From this analysis, it was possible to estimate the calcination temperature. Therefore, our data indicate that a more rough and porous V_2O_5 structure is obtained after calcination at 350 °C, as observed in the SEM image.

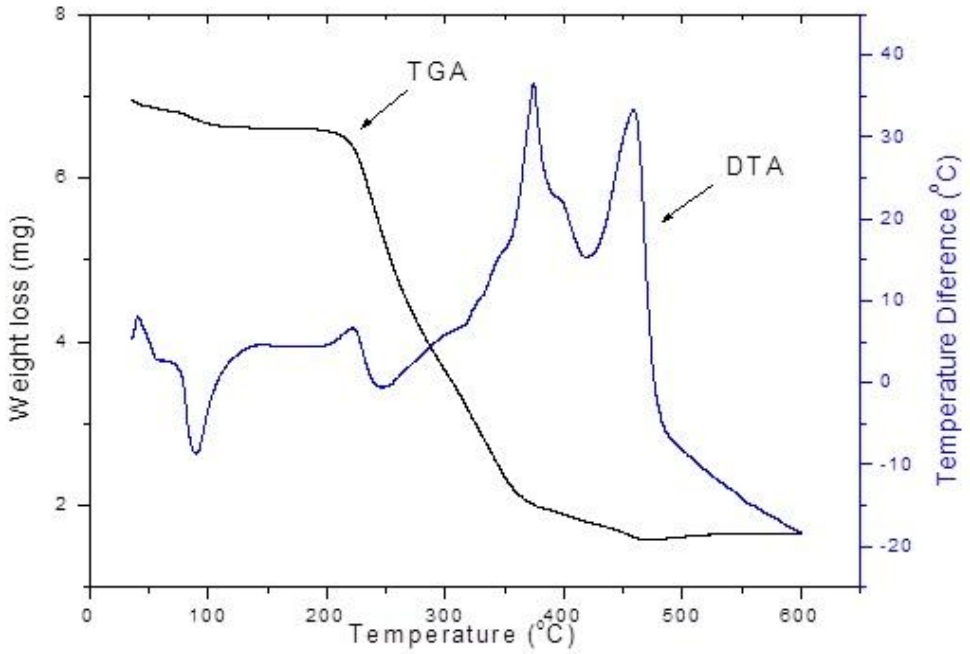

Figure 1. Thermogravimetric curve of VC1

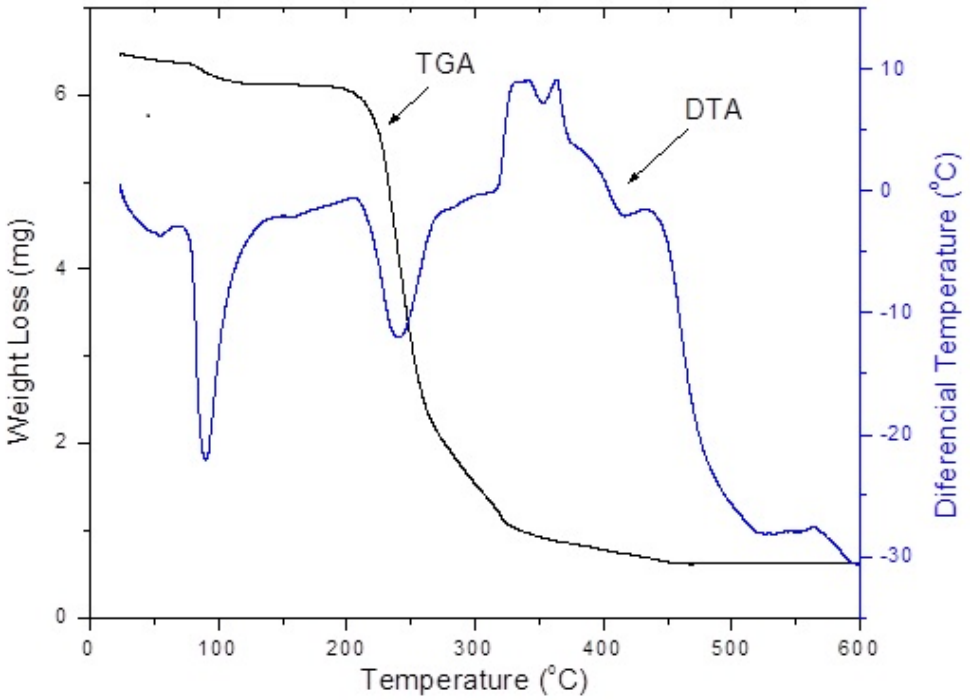

Figure 2. Thermogravimetric curve of VC2

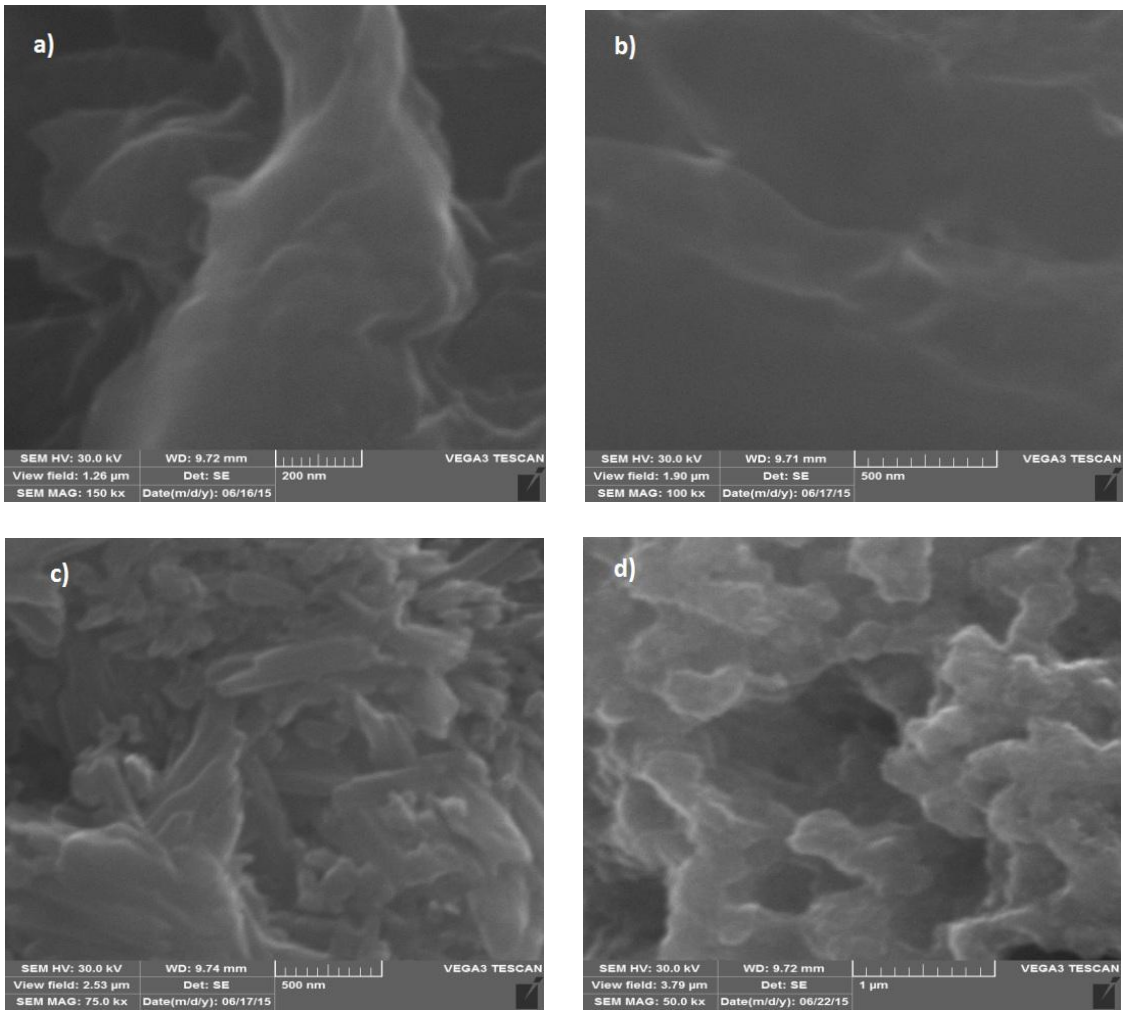

Figure 3. Scanning electron micrographs of (a) VC1, (b) VC2, (c) V1 and (d) V2

Based on images obtained from SEM, it was possible to estimate the changes of surfaces morphologies (Fig. 3a-d). The SEM images of VC1 and VC2 (Fig. 3a-b) present a more homogeneous surface compared to V1 and V2. The release of CPC from V_2O_5 caused a change in the final surface morphology. It is possible to note, in Fig. 3c-d, a formation of the more heterogeneous surface revealing reentrances that indicate the possible formation of a porous material. This change can provide an increase of surface area and a direct influence on the electrochemical response.

Fig. 4(a-b) depicts the XRD pattern of VC1 and VC2. It can be seen from Fig. 4, that the peaks could be related to the intercalation reaction of CPC into the layers of V_2O_5. Despite the surfactant was carried out in two different concentrations, the interlayer distance of VC1 and VC2 presented similar values. For both concentrations of CPC were observed an increase of d-spacing compared to V_2O_5 xerogel, from 1.17 nm, as described by our group [4], to 1.42 nm and 1.43 nm for VC1 and VC2, respectively. Additionally, the intense peak in (001) plane is typical of one dimensional stacking of the V_2O_5 xerogel ribbons perpendicular to the substrate [20]. Besides, diffraction patterns of the VC1 and VC2 showed the presence of narrow peaks, suggesting that these materials have high crystallinity, compared to V_2O_5 xerogel, as well as a bi-dimensional structure similar to that matrix. It is possible to note that the interlayer structure is maintained after intercalation reaction. This fact is observed by the

presence of diffraction peaks in (001), (002), (003), (004) and (005) planes. Moreover, other diffraction peaks were observed. Although the interlayer spacing of VC1 and VC2 are similar, the VC2 presents a high crystallinity compared to VC1 diffraction peaks. This difference can be due to the CPC molecules which remains more organized into the layer of the V_2O_5 xerogel. Also, it is possible to point out that the presence of CPC can be promoting the formation of two phases or domains in the same intercalation compound. This fact can indicate that the CPC molecules are reassembling in an intermittent way, consequently, giving rise to two domains [7].

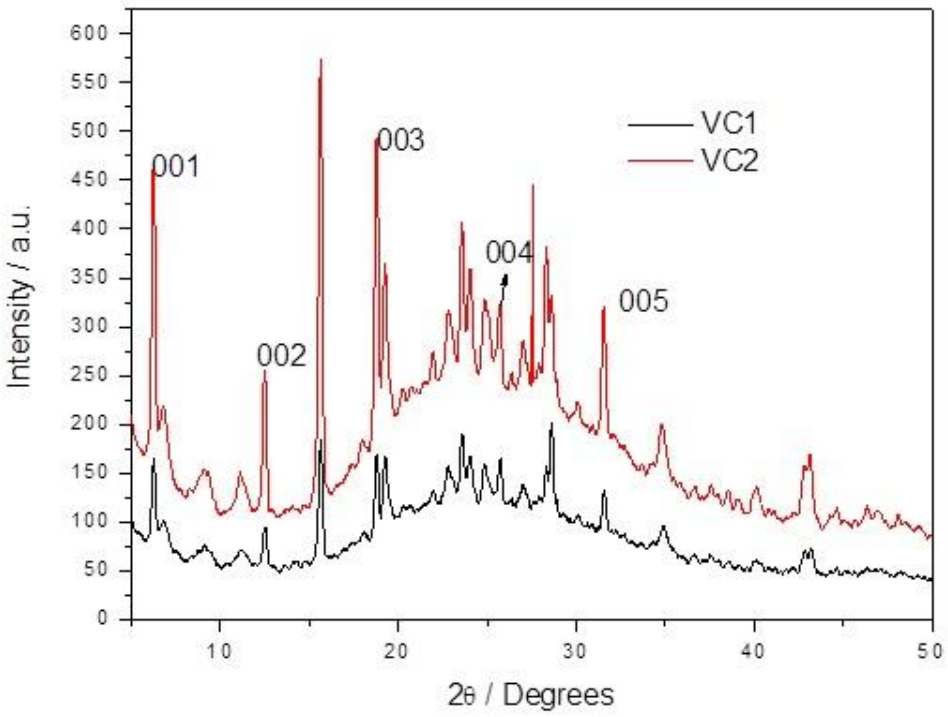

Figure 4. X-ray diffraction patterns of the samples: VC1 and VC2

After calcination, the lamellar structure of V_2O_5 has changed to another phase. The XRD pattern of V1 and V2 (Fig 5a-b) can be indexed to the orthorhombic phase of both samples and presenting higher crystallinity for V2. As comparison, in Fig. 5(c) is presented the XRD pattern for the V_2O_5 orthorhombic obtained commercially. It is possible to note from Fig 5. (a-b) that the driffractograms are quite similar to the diffractograms from Fig. 5(c), thus confirming the formation of the orthorhombic phase in V1 and V2. Figs. 6-8 present the cyclic voltammetry (CV) curves of V1, V2 and V_2O_5 xerogel, respectively. The CVs of V_2O_5 xerogel, V1 and V2 present peaks in the potential range of -1.5 V to +2.0 V (SCE), in acetonitrile solution containing 0.1 mol L^{-1} $LiClO_4$. It is possible to observe in Fig. 6-8 the cathodic and anodic peaks, ascribed to the $V^{V/IV}$ redox pair with the concomitant occurrence of lithium ion insertion and deinsertion ($xe^- + xLi^+ + V_2O_5.nH_2O \leftrightarrows Li_xV_2O_5.nH_2O$). After several cycles is possible to note the decrease of total charge. This fact can be associated with modifications in the structure during the insertion/deinsertion process.

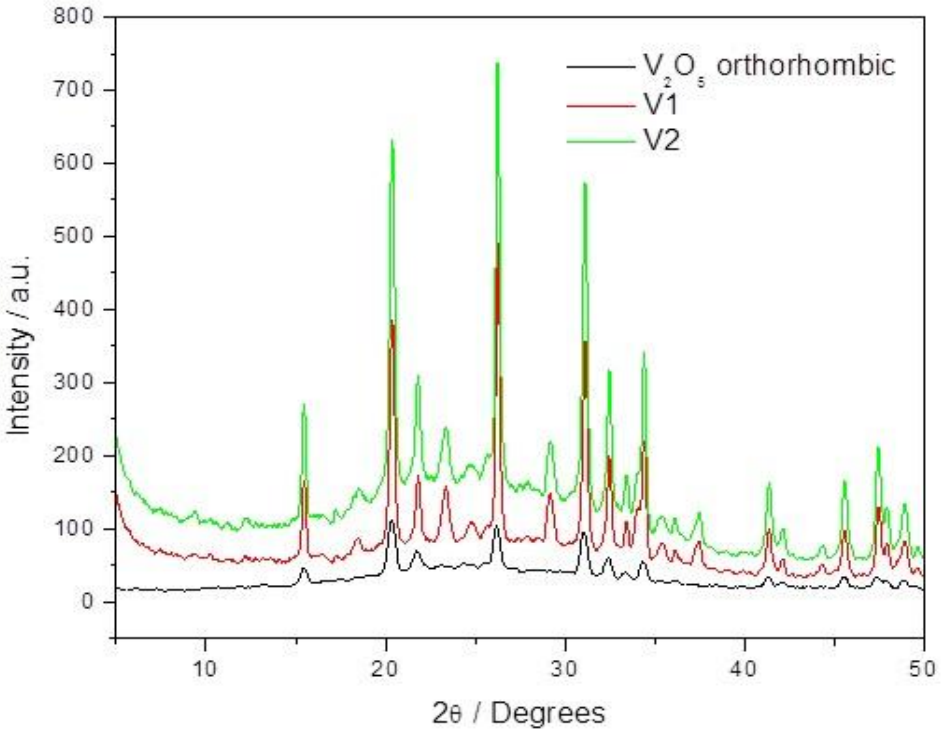

Figure 5. X-ray diffraction patterns of the samples: V_2O_5 orthorhombic (black line), V1 (red line) and V2 (green line)

The higher reduction of total charge occurs between the 1st to 15th cycle being verified a decreasing of 84%. After 15th cycle, the total charge begins to stabilize in a value nearly of 3 mC for V_2O_5 xerogel and V1 (Fig. 9). For V2 is possible to note a higher total charge value compared to V_2O_5 xerogel and V1, which begins to stabilize after the 25th cycle. This can be due to the fact that V2 presents an open and more heterogeneous structure containing reentrances on the surface. The presence of an open network promotes more facility for the Li^+ ions diffusion thus increasing the total charge. Moreover, the total charge difference between V1, V2 and V_2O_5 xerogel is perhaps due to the difficult lithium ion diffusion through the xerogel film arising from the steric hindrance conferred by the more compact structure [4] compared to V1 and V2 as observed in SEM images. As already quoted, the presence of a porous structure allows the reduction of the length of the diffusion path and provides a higher amount of active sites in the oxide network. Concerning the reduction of peak definition observed after several cycles in every case, this can be associated to the lithium ions insertion/deinsertion process, which is probably due to the generation of a stable Li$x$$V_2O_5$ crystalline phase, making the release of lithium ions into the supporting electrolyte solution more difficult [19]. Furthermore, during the redox reaction where the lithium ion insertion/deinsertion process takes place, can occur a contraction and expansion into the V_2O_5 lattice. Consequently, these structural changes after several charge/discharge cycles lead to irreversible structural changes in the material containing V_2O_5.

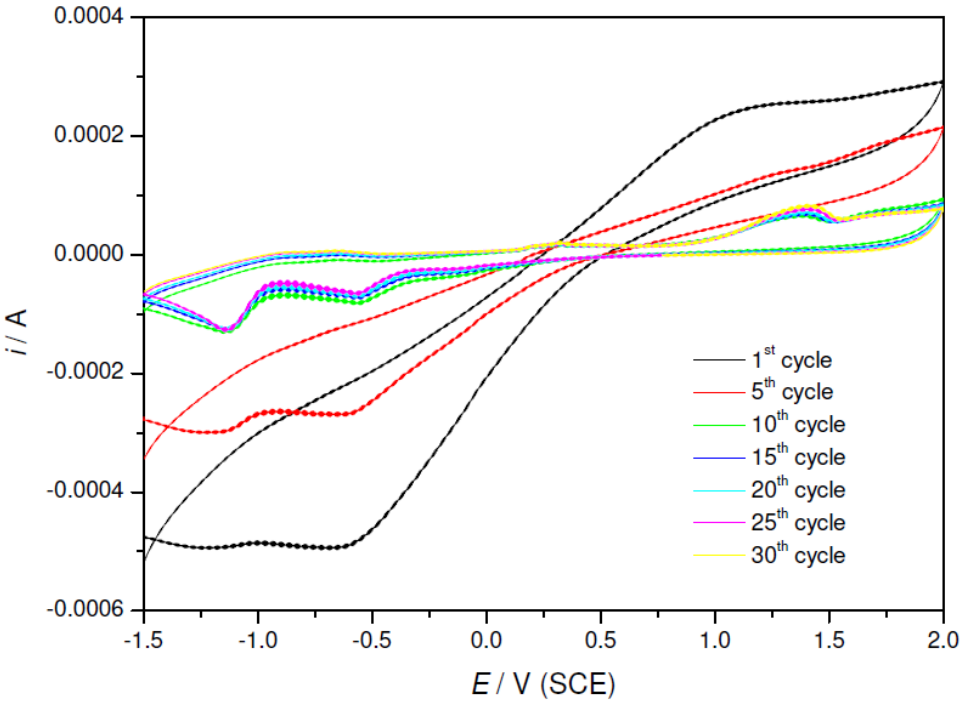

Figure 6. Cyclic voltammograms of the V1

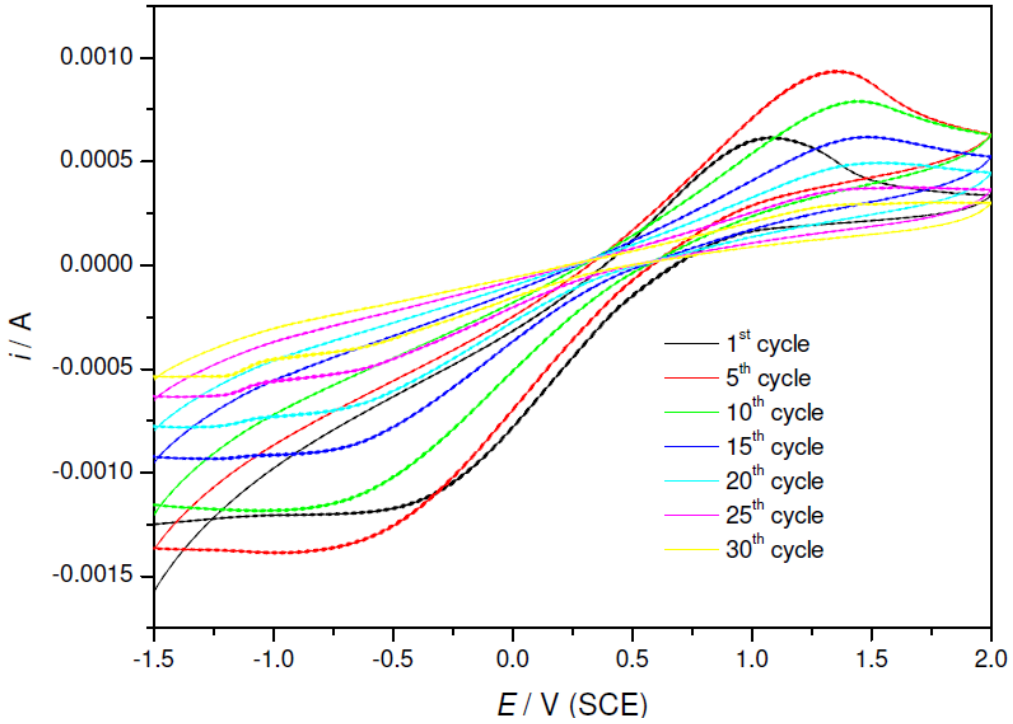

Figure 7. Cyclic voltammograms of the V2

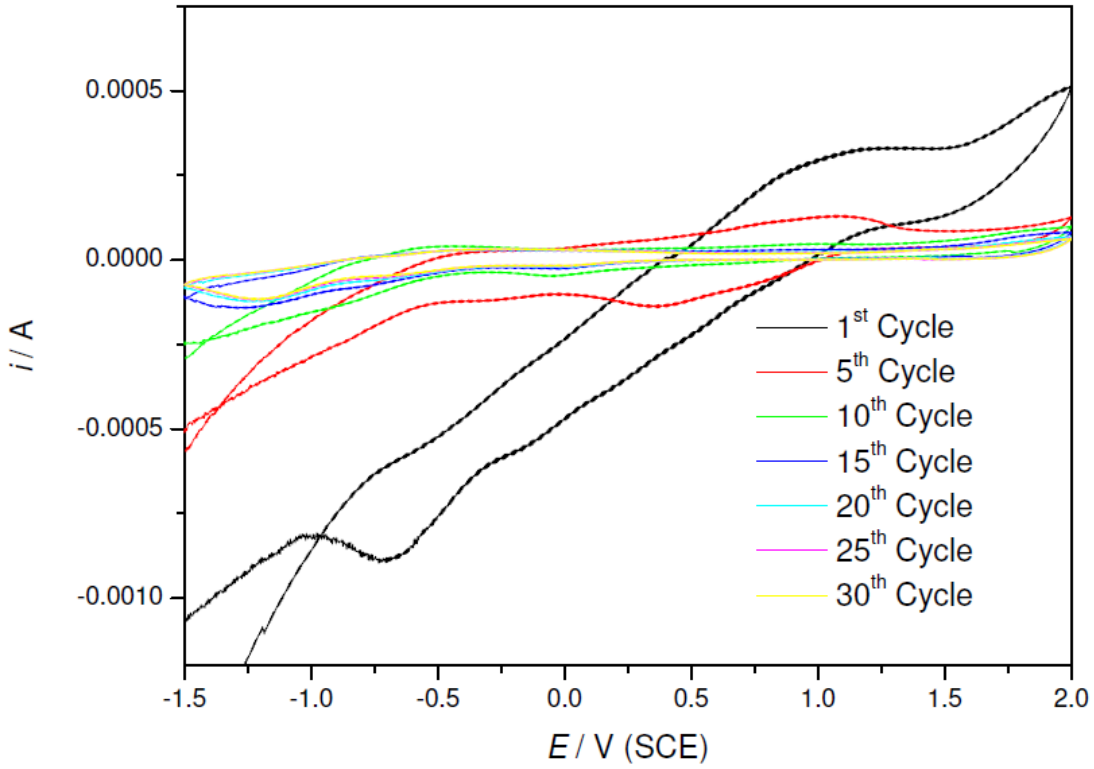

Figure 8. Cyclic voltammograms of the V_2O_5 xerogel

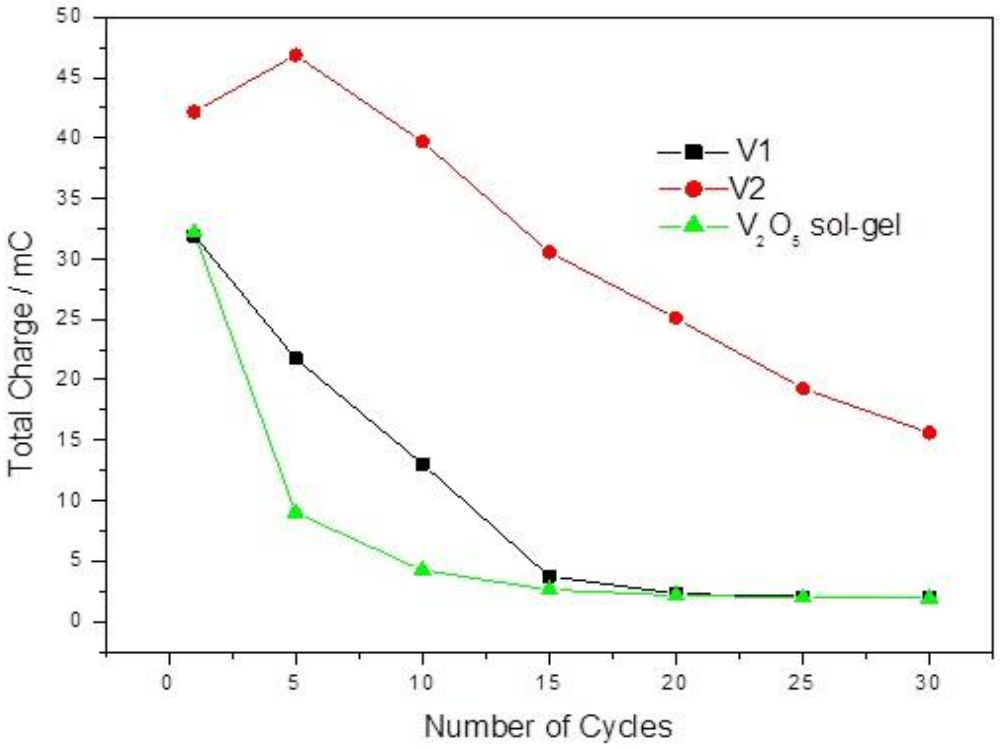

Figure 9. Cycle number in function of total charge of (■)V1, (●)V2 and (▲)V_2O_5 xerogel

4. CONCLUSIONS

Two different structures of V_2O_5 were synthesized by sol-gel route and by calcination process. The major effects obtained by different synthesis were evaluated and investigated by structural (XRD), morphological (SEM) and electrochemical (CV) characterization. The results concerning the structural and morphological characterization demonstrated that an intercalation reaction of CPC into the vanadium pentoxide matrix has occurred and the lamellar structure of the matrix was preserved. After calcination of VC1 and VC2 hybrids materials, the orthorhombic phase with higher crystallinity was obtained. The V2 structure presented a higher total charge as a consequence of the presence of a higher amount of actives sites, as well as the formation of an open network oxide structure.

ACKNOWLEDGEMENT
The authors gratefully acknowledge the fellowship provided by CAPES, FAPESP, FAPEMIG, INEO and CNPq are also acknowledged for financial support. Additionally, this work has also a collaboration research project of members of the Rede Mineira de Química (RQ-MG) supported by FAPEMIG (Project: CEX - RED-00010-14)

References

1. P. G. Bruce, *Solid State Science*, 7 (2005) 1456–1463.
2. P. G. Bruce, *Solid State Ionics*, 179 (2008) 752–760.
3. J. Shen, H. Wang, Y. Zhou, N. Ye, Y. Wang, L. Wang, *Chemical Engineering Journal*, 228 (2013), 724–730.
4. E. M. Guerra, D. T. Cestarolli, H. P. Oliveira, *Journal of Sol-Gel Science and Technology*, 54 (2010) 93–99.
5. G. E. Silva, K. V. S. Oliveira, R. F. Bianchi, D. T. Cestarolli, E. M. Guerra, *IEEE 42nd Photovoltaic Specialist Conference (PVSC)*, (2015) 1-4.
6. J. Schoonman, H. L. Tuller, E. M. Kelder, *Journal of Power Sources*, 81 (1999) 44-48.
7. E. M. Guerra, D. T. Cestarolli, L. M. da Silva, H. P. Oliveira, *Journal of Solid State Electrochemistry*, 14 (2010) 305-312.
8. F. Huguenin, E. M. Girotto, R. M. Torresi, D. A. Buttry, *Journal of Electroanalytical Chemistry*, 536 (2002) 37-45.
9. G. Picardi, F. Varsano, F. Decker, U. O. Krasovec, A. Surca, B. Orel, *Electrochimica Acta*, 44 (1999) 3157-3164.
10. A. Surca, B. Orel, U. O. Krasovec, U. L. Stangar, G. Drazic, *Journal of Electrochemistry Society*, 147 (2000) 2358-2378.
11. M. S. Whittingham, *Chemical Review*, 104 (2004) 4271-4301.
12. M. S. Whittingham, Y. Song, S. Lutta, P. Y. Zavalij, N. A. Chernova, *Journal of Materials Chemistry*, 15 (2005) 3362-3379.
13. E. M. Guerra, G. R. Silva, M. Mulato, *Solid State Sciences*, 11 (2009) 456-460.
14. E. M. Guerra, H. P. Oliveira, *Journal of Sol-Gel Science and Technology*, 50 (2009) 103–110.
15. E. M. Guerra, C. A. Brunello, C. F. O. Graeff, H. P. Oliveira, *Journal of Solid State Chemistry*, 168 (2002) 134–139.
16. E. M. Guerra, D. T. Cestarolli, H. P. Oliveira, *International Journal of Engineering Research and Application*, 4 (2014) 139-143.

17. X. Ren, C. Shi, P. Zhang, Y. Jiang, J. Liu, Q. Zhang, *Material Science and Engineering*, 177 (2012) 929–934.
18. Z. S. Chao, E. Ruckenstein, *Langmuir*, 19 (2003) 4235-4245.
19. E. M. Guerra, K. J. Ciuffi, H. P. Oliveira, *Journal of Solid State Chemistry*, 179 (2006) 3814–3823.
20. J. Livage, *Chemistry of Materials*, 3 (1991) 578–593.